

Synthesis, Characterization and Pyrolysis Kinetics of Chitosan-*N*-Phenylacetamide in an Ionic Liquid 1-Butyl-3-Methylimidazolium Chloride

Lahcen El Hamdaoui ^{1,*}, Maryam El Marouani ², Fatima Kifani-Sahban ³,
Mohammed El Moussaouiti ¹

¹ Laboratory of Materials, Nanotechnology and Environment, Center of Materials Sciences, Faculty of Sciences, Mohammed V University in Rabat, Morocco; la.elhamdaoui@gmail.com (L.E.H.);

² Department of Chemistry, College of Sciences, University of Hafr Al Batin, Hafr Al Batin, Kingdom of Saudi Arabia; melmarouani@uhb.edu.sa (M.E.M.);

³ Team of Modeling and Simulation of Mechanical and Energetic, Physical Department, Faculty of Sciences, Mohammed V University in Rabat, Morocco; kifani_sahban@yahoo.fr (F.K.S.);

* Correspondence: la.elhamdaoui@gmail.com;

Scopus Author ID 57190738516

Received: 25.08.2020; Revised: 7.10.2020; Accepted: 10.10.2020; Published: 14.10.2020

Abstract: This study intends to synthesis novel compound phenolic chitosan-based via reaction of chitosan with 2-Chloro-*N*-phenylacetamide in 1-butyl-3-methylimidazolium chloride ionic liquid in the presence of pyridine at 80 °C for 4 h. The alterations in the chemical structure and morphology of the chitosan-*N*-phenylacetamide biopolymer were verified using IR spectroscopy, XRD, and SEM analyses. Chitosan and Chitosan-*N*-phenylacetamide were subjected to thermo-gravimetric analysis under an inert atmosphere in the temperature range of room temperature - 600 °C at a heating rate of 20 °C.min⁻¹. The kinetic parameters were determined by the Coats-Redfern method. The corresponding kinetic parameters of the main degradation stages were also determined. The energy required for the degradation of pure chitosan was lower than that of chitosan-*N*-phenylacetamide in the first region of thermal degradation where the main pyrolysis reaction took place, and the largest weight loss occurred. Energy values in this region are running from 40.25 to 151.07 kJ/mol and 58.45 to 210.99 kJ/mol, respectively. The most probable reaction functions have thus been determined for these two stages by Coats-Redfern and Criado method, leading to greatly improved calculation performance over the entire conversion range. The pyrolysis reaction models of both pure chitosan and chitosan-*N*-phenylacetamide are described by the reaction, second-order F2.

Keywords: Chitosan; Chitosan-*N*-phenylacetamide; Ionic liquid; Coats Redfern.

© 2020 by the authors. This article is an open-access article distributed under the terms and conditions of the Creative Commons Attribution (CC BY) license (<https://creativecommons.org/licenses/by/4.0/>).

1. Introduction

Chitosan is a linear polysaccharide of $\beta(1-4)$ linked D-glucosamine. Due to its excellent characteristics, such as non-toxicity, biodegradability, and biocompatibility, chitosan has increasingly been used in diverse fields such as biomedical, environmental protection, agriculture, functional food, wastewater purification, and biotechnology [1-5]. It is easily obtained by the deacetylation of chitin; the second abundant biopolymer found on the earth obtained from shells of crustaceans such as crab, shrimp, and insects [1, 6, 7]. The process extraction of chitin is realized in two steps, deproteinization followed by demineralization [8, 9]. Chitosan and cellulose have the same chemical structure, except for an amine group (-NH₂)

at C-2 position instead of a -OH group for cellulose at this position [8]. The chitosan is a basic polysaccharide, whereas most biopolymers such as cellulose and dextran are either neutral or acidic in nature [1]. Chitosan has both reactive amino at C-2 position and -OH groups at C-3 and C-6 position, which can be used to chemically modification its physicochemical properties under mild reaction conditions [10, 11]. Due to the presence of amino groups in its structure, several chemical modifications are possible, such as the reaction with aldehydes and ketones to synthesis Schiff bases [12-15]. Chitosan can bind materials such as cholesterol, proteins, and tumor cells. It has also shown an affinity for proteins, such as wheat germ agglutinin and trypsin.

Ionic liquids (ILs) have an established ability to be used as replacements for dipolar aprotic solvents and have attracted much research attention because of their particular physicochemical properties, including thermal stability, non-volatility, non-flammability, and ease of recycling [16-18]. The ILs have the ability to dissolve polymers such as cellulose with different degree of polymerization [19-21] and chitosan [22-24]. The focus of recent research has been on the dissolution and regeneration of chitosan by its dissolving in 1-butyl-3-methylimidazolium chloride [Bmim](Cl) ionic liquid [25].

The kinetics of degradation of materials is essential for investigating the thermal stability of compounds. Thus, it is very practical to understand the mechanisms controlling the interaction between chemical and physical processes. The thermogravimetric analysis is one of the simplest and popular techniques that can be used to study the Degradation kinetics of biopolymers [26]. For several years, great effort has been devoted to the study of characteristics of thermal degradation, including kinetic parameters on pure and modified chitosan under inert and oxidative atmospheres [26]. Thus, a wide range of values for chitosan kinetic parameters has been reported in the literature [27-30].

The 2-chloro-*N*-phenylacetamide is a flavoring compound and a bioactive agent, which can be used as antimicrobial agents such as herbicides, antifungal, disinfectant [31, 32], creating the possibility of obtaining new chitosan-based biopolymer with improved properties. We have previously reported the synthesis of cellulose-acetanilide ethers with different degrees of substitution, and its antibacterial activity were tested against the bacterium *Rhodococcus* sp. GK1 [33].

They are taking all these into account, this paper addressing the synthesis and characterization of chitosan-*N*-phenylacetamide biopolymer with potential applications. To reach this target, the 2-chloro-*N*-phenylacetamide is reacted with chitosan in an IL [Bmim](Cl) in the presence of pyridine at 80 °C for 4 h under the mild reaction conditions. The synthesized biopolymer was analyzed by IR, XRD, thermogravimetric analysis (TGA-DTG), and scanning electron microscopy (SEM). In addition, the kinetic parameters are determined by the Coats Redfern method.

2. Materials and Methods

2.1. Materials.

Chitosan from shrimp shells with a degree of deacetylation of 75% was purchased from Sigma-Aldrich. 2-Chloro-*N*-phenylacetamide and 1-butyl-3-methylimidazolium chloride ([Bmim]Cl) IL were synthesized in Laboratory [31, 34] with a slight of modification. Pyridine and Methanol (MeOH) were purchased from Aldrich chemical and used without further purification.

2.2. Methods of materials analyzes.

2.2.1. Infrared characterization.

The apparatus used for infrared spectroscopy characterization is a Bruker-Tensor 70, which operates in transmittance mode. This apparatus is equipped with a Globar source that emits radiation in the region of mid-infrared and of a DLaTGS detector. The acquisition is between 4000 and 400 cm^{-1} in wavenumber. The number of scans is 20, with a resolution of 4 cm^{-1} . The infrared absorption spectrum was recorded from a sample in a solid form prepared as pellets to 1% by weight of product dispersed in KBr.

2.2.2. X-ray diffraction (XRD).

X-ray diffraction is an effective way to study the crystallinity and structuration of the biopolymer samples. Herein the spectra were obtained at room temperature with a powder diffractometer LABXXRD-6100 SHIMADZU equipped with a monochromatic $\text{Cu K}\alpha$ (1.5418 Å) X-ray source at a voltage of 50 kV. The samples were analyzed in a continuous mode over an angular range of 5 - 35° with a step size of 0.02° and a scanning time of 2 seconds by step.

2.2.3. Scanning electron microscopy (SEM) analyses.

The morphology of the pure chitosan and the chitosan-*N*-phenylacetamide were characterized by scanning electron microscopy (SEM), using a FEI Quanta 200 microscope. The samples were coated with a carbon layer to increase their conductivity and analyzed at an accelerating voltage of 30 kV.

2.2.4. Thermogravimetric and differential thermal analyzes.

The simultaneous thermal analyzer of the 'LabsysTMEvo (1F)' type and SETARAM brand was used for the thermogravimetric (TG), and thermal differential analyses (DTA) of pure and modified chitosan under an inert atmosphere at a flow rate of 10 $\text{cm}^3\cdot\text{min}^{-1}$. This apparatus consists of a TG microbalance associated with DTA sensor with a single rod, a metal resistor furnace up to 1600 °C, and multitasking software controlling the various modules. 10 mg of the sample was taken in the ceramic sample holder to ensure the uniformity of temperature in the range 30–600 °C at a heating rate of 20 °C $\cdot\text{min}^{-1}$. Three replicates were made for TG and DTA of each sample biopolymer.

2.3. Dissolution of Chitosan in IL [Bmim](Cl).

0,3 g of chitosan was mixed with 9,7 g of [Bmim](Cl) in a two-neck round-bottom flask. This heterogeneous mixture was stirred at 130 °C for a maximum of 4 h to obtain a 5 wt% homogeneous chitosan solution. The solubility of chitosan was checked visually.

2.4. Synthesis.

The chitosan-*N*-phenylacetamide was synthesized as follows: First, pyridine (2 mL) was added portion-wise to a flask containing chitosan/[Bmim](Cl) solution at 40 °C over 1 h with stirring. Upon the addition of pyridine, the mixture became less viscous. Next, 300 mg of 2-Chloro-*N*-phenylacetamide was added in small amounts. After every addition of 2-Chloro-*N*-phenylacetamide, the flask was vigorously agitated. Four hours were allowed for the reaction

to proceed at 80 °C under magnetic stirring. After cooling the solution to room temperature, the polymer was precipitated in 100 mL of ethanol. The obtained product chitosan-*N*-phenylacetamide was filtered and washed several times with methanol and then dried at 40 °C in a vacuum for 2 hours. The obtained product with a computed % yield of 81% if the theoretical yield is calculated for a degree of substitution of 1.

2.5. Kinetic approach.

There are several approaches for estimating kinetic parameters from thermogravimetric data. It is, therefore, essential to specify the approach adopted in any kinetic exploitation of the experimental mass loss data. In this work, the kinetic parameters are determined by the Coats Redfern method. The procedure for determining kinetic parameters using this method is presented in section 2.5.1. The expression to achieve these parameters is obtained from the reaction rate. Thus, in the kinetic analysis of thermal decomposition reactions, the reaction rate is written according to the following form:

$$\frac{d\alpha}{dt} = kf(\alpha) \quad (\text{Eq.1})$$

Where, α is a characteristic variable of reaction progress, related to the mass of the sample m by the formula:

$$\alpha = \frac{m_0 - m_t}{m_0 - m_f} \quad (\text{Eq.2})$$

Where, m_0 is the initial weight of the sample, m_t is the weight of the sample at the particular temperature T , and m_∞ is the weight at the end of the degradation step.

$f(\alpha)$ represent the mode of degradation of the substance. The function $f(\alpha)$ does not depend on the temperature but rather on the degradation model of the subject matter.

The different modes proposed in the literature [35-37] are grouped in table 1. In this same table, the function

$$g(\alpha) = \int_0^\alpha \frac{d\alpha}{f(\alpha)} \quad \text{represents the integral form of the function } f(\alpha) \quad [38]$$

k is the reaction rate constant. It is accepted that k following the Arrhenius law:

$$k = A \exp\left(\frac{-E}{RT}\right) \quad (\text{Eq.3})$$

Where E is the apparent activation energy in $\text{kJ}\cdot\text{mol}^{-1}$, R is the perfect gases constant in $\text{J}\cdot\text{K}^{-1}\cdot\text{mol}^{-1}$, A is the pre-exponential factor or frequency factor in min^{-1} , T is the absolute temperature in °K, A , E , and $f(\alpha)$ are called the kinetic triplets of a reaction. Substitution of Eq.3 in Eq.2 gives:

$$\frac{d\alpha}{dt} = Af(\alpha)\exp\left(\frac{-E}{RT}\right) \quad (\text{Eq.4})$$

For a specific solid-state reaction, the expression of $f(\alpha)$ depends on the reaction mechanism.

Table 1. Thermal degradation modes proposed for gas-solid reactions.

| Degradation mode | Code | Differential form : f(α) | Integral form : g(α) |
|---|------------|---|---|
| Diffusion | | | |
| One-way transport | D1 | 1 / (2α) | α ² |
| two-way transport , Valensi-Barrer [38] | D2 | -1 / Ln(1-α) | α + (1-α)Ln(1-α) |
| three-way transport, Jander [40] | D3 | 1,5(1-α) ^{2/3} / [1-(1-α) ^{1/3}] | [1-(1-α) ^{1/3}] ² |
| Ginstling-Brounshtein [41] | D4 | 1,5 / [(1-α) ^{-1/3} -1] | 1-2α/3-(1-α) ^{2/3} |
| Zhuravlev | D5 | 1,5(1-α) ^{2/3} / [1 / (1-α) ^{1/3} -1] | [1 / (1-α) ^{1/3} -1] ² |
| Anti-Jander | D6 | 1,5(1+α) ^{2/3} / [(1+α) ^{1/3} -1] | [(1+α) ^{1/3} -1] ² |
| Kroger-Ziegler | D7 | [1,5(1-α) ^{2/3} / [1-(1-α) ^{1/3}]] / t | [1-(1-α) ^{1/3}] ² - log(t) |
| Two dimensions, Jander | D8 | (1-α) ^{1/2} / [1-(1-α) ^{1/2}] | [1-(1-α) ^{1/2}] ² |
| Two dimensions, Anti-Jander | D9 | (1+α) ^{1/2} / [(1+α) ^{1/2} -1] | [(1+α) ^{1/2} - 1] ² |
| Interfacial transfer | D10 | 3(1-α) ^{4/3} | [1/ (1-α) ^{1/3} - 1] |
| Transfer and diffusion | D11 | 3 / [(1-α) ^{-4/3} - (1-α) ⁻¹] | 1/(1-α) ^{1/3} -1+1/3Ln(1-α) |
| Diffusion with two directions | D12 | 3 / [(1-α) ^{-8/3} - (1-α) ^{-7/3}] | 1/5(1-α) ^{-5/3} - 1/4(1-α) ^{-4/3} +1/20 |
| Random nucleation and nuclei growth | | | |
| Avrami-Erofeev [42, 43] n = 1, 2, 3, 4 et 5 | An | x(1-α)[-Ln(1-α)] ^y x=4, 2, 3, 4/3 and 3/2 y=3/4, 1/2, 2/3, 1/4 and 1/3 | [-Ln(1-α)] ^z z=1/4, 1/2, 1/3, 3/4 and 2/3 |
| Chemical reactions | | | |
| Zero order | F0 | Constant | α |
| First order | F1 | 1-α | -Ln(1-α) |
| Second order | F2 | (1-α) ² | (1-α) ⁻¹ -1 |
| Contraction (surface, volume and interface respectively for n = 2, 3 and 4) | Rn | x(1-α) ^y x=2, 3 et 3/2. y=1/2, 2/3 and 1/3 | 1-(1-α) ^z z = 1/2, 1/3 and 2/3 |
| Power / Exponential | | | |
| Low power (half, third and quarter respectively for n = 2, 3 and 4) | Pn | nα ^x x = 1/2, 2/3 and 3/4 | α ^y y = 1/2, 1/3 et 1/4 |
| Exponential | | | |
| | E1 | α | Ln(α) |

D₁, D₂,...are symbols given to models.

2.5.1. Procedure for kinetic parameter determination.

In order to determine kinetic parameters of pure and modified chitosan samples, the Coats–Redfern method [26, 44-45], which is given Eq.5, is expressed as follows:

$$\text{Ln} \left(\frac{g(\alpha)}{T^2} \right) = \text{Ln} \frac{AR}{\beta E_\alpha} - \frac{E_\alpha}{RT} \quad (\text{Eq.5})$$

Where α is a characteristic variable of reaction progress of the sample, g(α) represents functions commonly used for the description of thermal decomposition (Table 1), and β is the heating rate.

A plot of Ln (g(α)/T²) against 1/T will give a straight line of slope -E_a/R and an intercept of Ln(AR/βE) for an appropriate form of g(α). Thus, based on the correct form of g(α), the activation energy and the pre-exponential factor could be respectively determined from the slope and intercept terms of the regression line.

2.5.2. Criado method.

If the value of the activation energy is known, the kinetic model of the process can be determined by the Criado method [46] method. Combining the Eq. (4) with Eq. (5), the following equation is obtained:

$$\frac{Z(x)}{Z(0.5)} = \frac{f(\alpha)g(\alpha)}{f(0.5)g(0.5)} = \left(\frac{T_x}{T_{0.5}} \right)^2 \frac{(dx/dt)_x}{(dx/dt)_{0.5}} \quad (\text{Eq.6})$$

Where 0.5 refers to the conversion in $x = 0.5$.

The left side of Eq. (15) $f(x)g(x)/f(0.5)g(0.5)$ is a reduced theoretical curve, which is characteristic of each reaction mechanism, whereas the right side of the equation associated with the reduced rate can be obtained from experimental data.

A comparison of both sides of Eq. (15) tells us which kinetic model describes an experimental reactive process. Table 1 indicates the algebraic expressions of $f(x)$ and $g(x)$ for the kinetic models used

Table 1 lists the most common kinetic $g(\alpha)$ functions, which were used in this study for the estimation of reaction mechanisms from dynamic TG curves by using the Coats–Redfern method.

For both studied samples, all of the mechanisms in Table 1 were tested, and calculation results were compared. The main purpose was to select the mechanism of the thermal degradation of chitosan samples.

3. Results and Discussion

3.1. Synthesis of chitosan-*N*-phenylacetamide.

The chitosan-*N*-phenylacetamide derivative was synthesized by the etherification reaction of -OH groups of the chitosan chains with 2-Chloro-*N*-phenylacetamide. The reaction was performed homogeneously in [Bmim](Cl) solvent at 80 °C for 4 h in the presence of pyridine. The reaction process for the synthesis of chitosan-*N*-phenylacetamide was shown in figure 1.

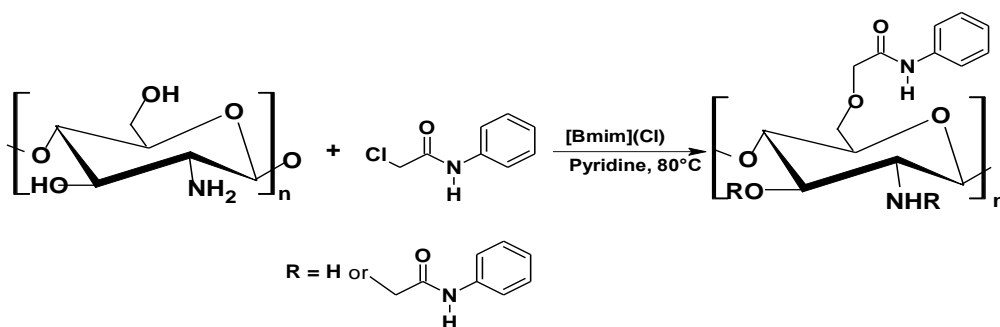


Figure 1. Reaction scheme for the synthesis of chitosan-*N*-phenylacetamide.

3.2. Characterization of samples.

3.2.1. Infrared characterization.

Figure 2 demonstrates the IR spectral analysis of pure chitosan (a) and chitosan-*N*-phenylacetamide derivative (b). The spectrum (a) showed the main characteristic broadband between 3200-3500 cm^{-1} , corresponding to the stretching vibration of amine (N-H) and hydroxyl (O-H) groups of polysaccharides. The peak appeared at 2920 cm^{-1} is attributed to the stretching vibration of CH, the peaks at 1650 and 1556 cm^{-1} assigned to amide (I). The band at 1374 cm^{-1} corresponding to NH_2 bend vibration. Further peaks appeared at 1072 and 1416 cm^{-1} are due to stretching vibration of C–O–C pairing in β (1 \rightarrow 4) glycosidic bonds of polysaccharide and C–N, respectively. On the other hand, the IR spectrum of chitosan-*N*-phenylacetamide (b) provide clear evidence of etherification by showing the strong characteristic absorption peaks at 3400 cm^{-1} for N–H stretching in amide and 847 cm^{-1} for C–N, the band at 1020 cm^{-1} refer to stretching vibration of (O–C–O ether), the bands at 1471 and

1560 cm^{-1} are attributed to deformation of C = C and C–H stretching of the aromatic ring, respectively. These results confirm the chemical modification of chitosan and the formation of a chemical bond between these compounds, confirming that the reaction of the hydroxyl group of chitosan with 2-Chloro-*N*-phenylacetamide in ionic IL [Bmim](Cl) in the presence of pyridine has occurred.

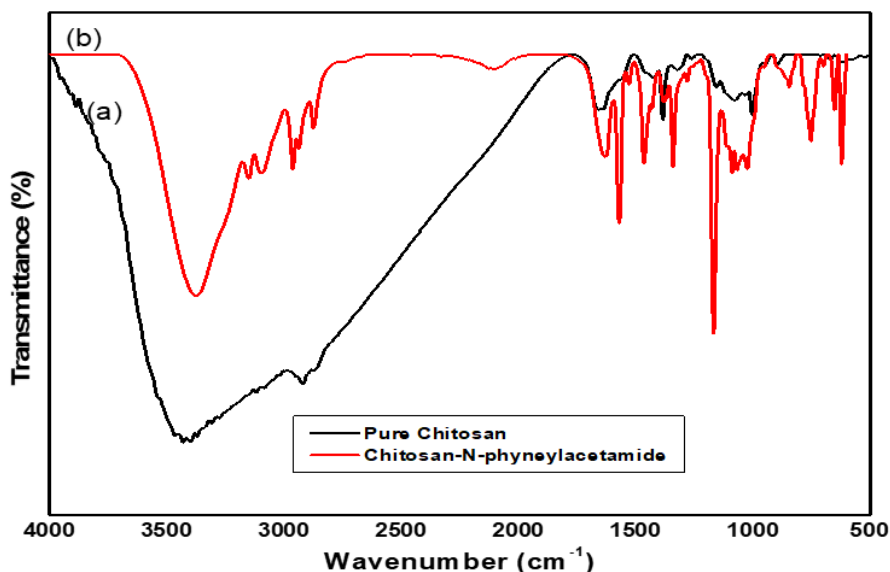


Figure 2. Infrared spectrum of chitosan and chitosan-*N*-phenylacetamide.

3.2.2. X-ray Diffraction (XRD) pattern.

Figure 3 shows the XRD patterns of pure chitosan and chitosan-*N*-phenylacetamide derivative. This XRD pattern of pure chitosan showed very broad peaks at $2\theta = 10^\circ$ and $2\theta = 20^\circ$ [47]. The chitosan-*N*-phenylacetamide displayed one peak at around 2θ of 20° . However, the peak observed for chitosan at $2\theta = 10^\circ$ disappeared, and the peak at $2\theta = 20^\circ$ became very broad in Chitosan-*N*-phenylacetamide derivative. These results showed good compatibility for chitosan.

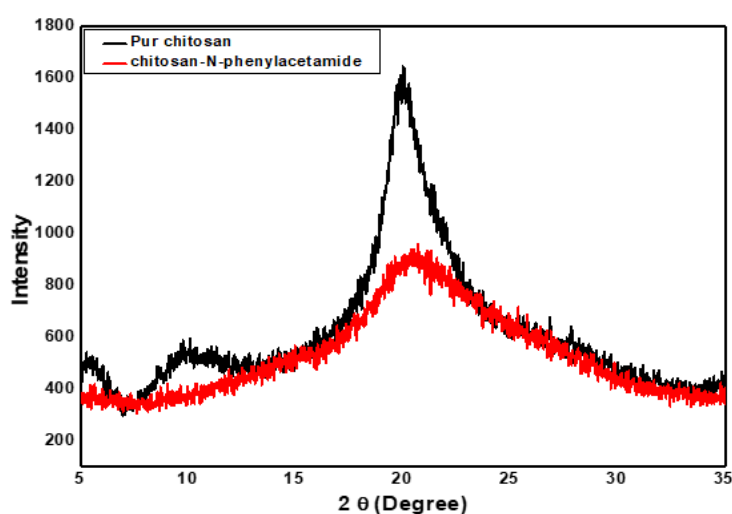


Figure 3. X-ray Diffraction spectra of pure chitosan and chitosan-*N*-phenylacetamide.

The crystallinity index (CI) was calculated from the following equation [48]:

$$\text{CI (\%)} = \frac{I_{\text{max}} - I_{\text{am}}}{I_{\text{max}}} \times 100$$

Where I_{\max} is the maximum intensity at $2\theta = 20^\circ$ and I_{am} is the intensity of amorphous diffraction at $2\theta \sim 16^\circ$ [49]. The calculated crystallinity index values were found to be 57.45 and 38.54% for chitosan and Chitosan-*N*-phyneylacetamide, respectively. From this, we deduce that the introduction of *N*-phyneylacetamide group leads to a change of crystallinity of chitosan and that this change is probably dependent on the other factors, such as special hindrance, hydrophobic force, and π - π stacking [50].

3.2.3. Scanning Electron Microscopy (SEM).

Figure 4 displays the morphological structure of chitosan (a) and chitosan-*N*-phyneylacetamide derivative (b). The SEM images of the surface of pure chitosan and chitosan derivative show clear differences between them. The pure chitosan is mainly composed of platelet-like chitosan micro-fibrils with a variable size. However, the surface structure of the chitosan derivative is compact and homogeneous; the surface roughness of the chitosan derivative was increased than pure chitosan. Interruption of the backbone of chitosan-*N*-phenylacetamide polymer can explain this observation as a result of the reaction of the hydroxyl group (-OH) of chitosan with 2-Chloro-*N*-phenylacetamide and probably due to breaking of hydrogen bonds present in the pure chitosan and interaction between the newly introduced hydrophobic phenyl groups. Thus, the reaction of chitosan with 2-Chloro-*N*-phenylacetamide leads to very significant changes in the surface morphology and crystallinity of the chitosan.

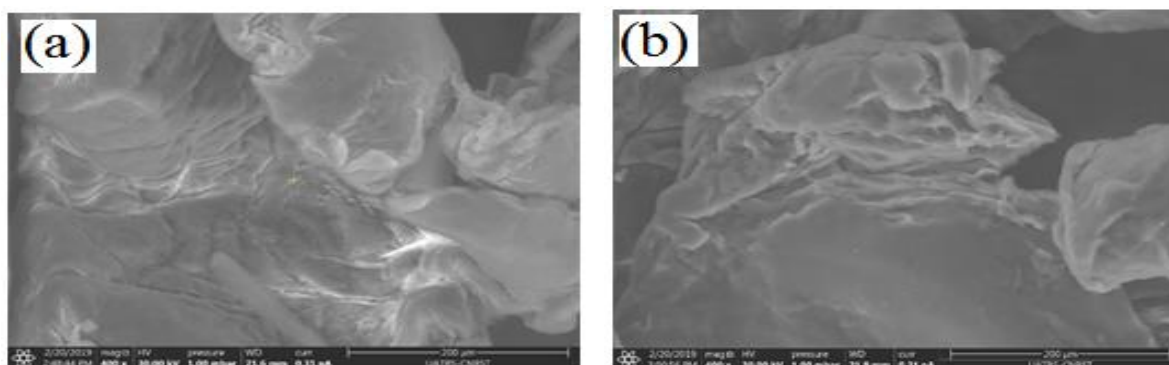


Figure 4. SEM microphotographs of pure chitosan (a) and chitosan-*N*-phenylacetamide derivative (b) (magnification: x 400).

3.4. Thermal profile under an inert atmosphere.

3.4.1. Thermogravimetric analysis (TGA-DTG).

The thermal behavior of pure chitosan and chitosan-*N*-phenylacetamide are presented in figure 5. The main thermal characteristics from the TGA-DTG curves such as the temperature of the beginning of the degradation process (T_0), the temperature of maximum mass loss (T_{\max}), and the percentages of carbon residue (CR %) both at T_{\max} and at 380°C are given in Table 2.

The TG and DTG curves obtained for chitosan and chitosan-*N*-phenylacetamide show two stages of weight loss, The first exhibit an initial small drop between 30 and 105°C with a weight loss of approximately 8%, the second with a weight loss of 41 and 51% for pure chitosan and chitosan-*N*-phenylacetamide, respectively. The first range, from room temperature to about

105 °C is relative to dehydration. This latter would be linked to the departure of the so-called free water of the material [51].

The second zone of thermal decomposition, from 240 to 380 °C for pure chitosan, corresponds to the main pyrolysis and to volatilization of compounds produced from the thermal degradation of polymeric chitosan chains. In this temperature range, the sharp peak has a maximum at 306 °C. This peak is surrounded on its left side by a shoulder, which is caused by the loss of functional groups of coupled chitosan [47]. Regarding chitosan-*N*-phenylacetamide second mass loss, from 190 to 380 °C, mass loss about 51%, with DTG peak centered at 253 °C. According to some authors [52-54], the first stage is connected with deacetylation and depolymerization of chitosan. The second one corresponds to the residual cross-liked degradation chitosan [54].

At the end of the thermal solicitation, the yield of solid residue, in this case, carbon residue at 380 °C and at T_{max} increased by 4 %, whereas T_{max} decreased by 50 °C, compared to T_{max} of the pure chitosan.

Thermogravimetric analysis shows that chitosan-*N*-phenylacetamide is less thermally stable than pure chitosan. This behavior may be related to the crystallinity of these materials. Indeed, chitosan-*N*-phenylacetamide has a lower crystallinity than pure chitosan (Figure 3).

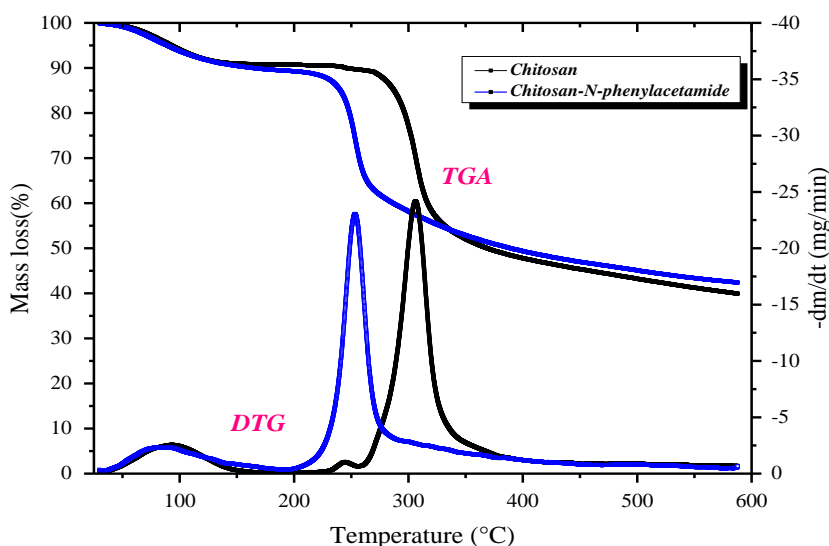


Figure 5. TGA and DTG temperature dependencies of chitosan and chitosan-*N*-phenylacetamide.

Table 2. Thermal characteristics of pure chitosan and chitosan-*N*-phenylacetamide derivative.

| Sample | T_0 (°C) | T_{max} (°C) | CR % (at T_{max}) ^a | CR % (at 400 °C) ^b |
|-------------------------------------|------------|----------------|--------------------------------------|----------------------------------|
| Chitosan | 240 | 306 | 70 | 48 |
| chitosan- <i>N</i> -phenylacetamide | 190 | 253 | 74 | 52 |

T_0 , temperature of the beginning of the degradation to 3% mass loss, T_{max} , temperature of maximum mass loss

^a Percentage of carbon residue at T_{max}

^b Percentage of carbon residue at 380 °C.

3.4.2. Differential thermal analysis.

The DTA thermogram obtained by the thermal degradation of pure chitosan and chitosan-*N*-phenylacetamide derivative at a heating rate of 20 °C.min⁻¹ is shown in figure 6.

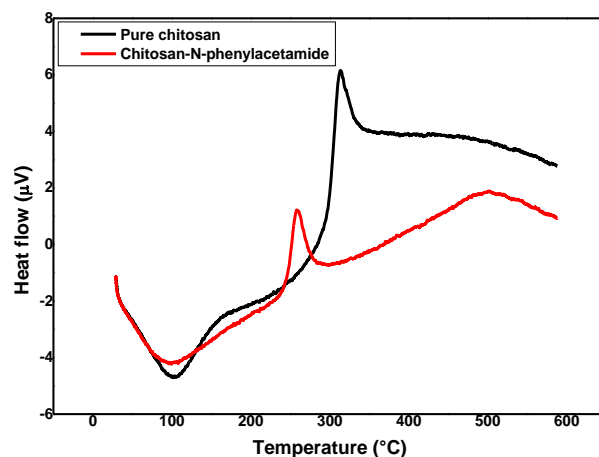


Figure 6. DTA plots of pure chitosan and chitosan-*N*-phenylacetamide.

The DTA thermogram of chitosan presents two broad peaks, the first one at about 100 °C was accompanied by an endothermic effect, may attribute to the evaporation of water absorbed in the inner chitosan chains, while the second is an exothermic peak at 313 °C may be due to the molecular arrangement of the polymer. DTA thermogram of chitosan-*N*-phenylacetamide derivative (Figure 6) showed characteristic sharp endothermic peaks at 100 °C due to the loss of water molecules. There is one broad exothermic peak at 258 °C corresponding to the thermal decomposition of chitosan-*N*-phenylacetamide. An offset of 55 °C is observed between the exothermic picks; it is maybe due to the change of the structure of the material and the change of the mechanism of its thermal degradation process due to the *N*-phenylacetamide compound and the reduced ability to crystallize.

3.4.3. Kinetic parameters estimation.

In order to calculate and understand the nature of the decomposition, kinetic exploitation is made on a dynamic chemical regime, assuming that the decomposition is a global reaction where the physical limitation is neglected. The complete thermogram was divided into distinct sections according to their degradation steps. Curves indicating the solid-state mechanisms of pure and modified chitosan degradation under an inert atmosphere are shown in figure 7. The values of activation energy E_a , pre-exponential factor A and correlation factors R^2 are listed in Tables 3 and 4, respectively, for the first and second degradation steps. Moreover, the parameters A and E are moving in the same direction, and their values depend on the mode of degradation. The relationship between A and E_a , called the “apparent compensation effect” is often mentioned in the literature. Figure 8 shows traces of the values of $\ln A$ as a function of E_a . The effect of compensation is another way to further discrimination between degradation modes. Thus, for the first region (second weight loss step in TGA thermogram), it was observed from table 3 that the best correlation coefficients were obtained for F0, F2, F3, R2, R3, P2, P3, D3, A2, and A3 for pure chitosan and F0, F1, F2, F3, R2, R3, P2, P3, D3, A2 and A3 for chitosan-*N*-phenylacetamid. In addition, the energy required for the degradation of pure chitosan is lower than that of chitosan-*N*-phenylacetamid, with energy values running from 40.25 to 151.07 kJ/mol and 58.45 to 210.993 kJ/mol, respectively. Regarding the second degradation step (third weight loss step), degradation mechanisms that give the best mathematical fit for both samples were F1, F2, F3, R3, and D3 with values of activation energy for pure chitosan close to that of chitosan-*N*-phenylacetamid.

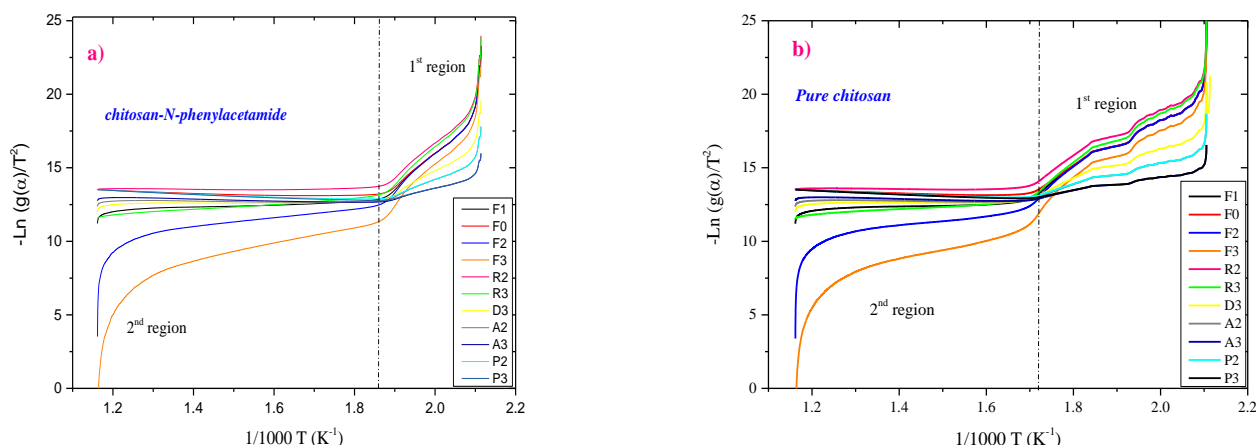


Figure 7. Curves indicating the solid-state mechanisms of pure and modified chitosan degradation under an inert atmosphere.

This indicates that the presence of *N*-phenylacetamide has an accelerating effect on the decomposition. Likewise, the results of the two regions show that the highest activation energies were found in the first thermal degradation regions where the main pyrolysis reaction took place, and the largest weight loss occurred. The values of the pre-exponential factor (Tables 3 and 4) indicate that it depends on the degradation mode.

There are differences between our kinetic parameters and those in literature reviews [27-30]. These differences can be attributed to the nature of chitosan and its degree of deacetylation, to different calculation methods, and to experimental conditions.

Table 3. Thermal kinetic results for Pure and modified chitosan first region of pyrolysis.

| DM | <i>Pure chitosan</i> | | | <i>Chitosan-N-Phenylacetamide</i> | | |
|-----------|----------------------|-------------------------|---------------------------|-----------------------------------|-------------------------|---------------------------|
| | R ² | E _a (kJ/mol) | Ln A (min ⁻¹) | R ² | E _a (kJ/mol) | Ln A (min ⁻¹) |
| F0 | 0.988 | 134.78 | 8.38 | 0.992 | 191.62 | 23.97 |
| F1 | - | - | - | 0.993 | 201.31 | 26.28 |
| F2 | 0.980 | 142.63 | 10.20 | 0.990 | 207.06 | 27.68 |
| F3 | 0.971 | 151.07 | 12.88 | 0.945 | 243.84 | 36.94 |
| R2 | 0.987 | 137.20 | 8.24 | 0.991 | 198.04 | 24.756 |
| R3 | 0.986 | 149.14 | 11.26 | 0.993 | 210.993 | 28.08 |
| P3 | 0.984 | 39.06 | 9.52 | 0.990 | 58.45 | 4.520 |
| D3 | 0.984 | 90.23 | 0.0019 | 0.993 | 131.78 | 11.134 |
| P2 | 0.986 | 62.99 | 5.214 | 0.991 | 91.90 | 2.473 |
| A2 | 0.983 | 64.76 | 4.818 | 0.992 | 96.58 | 3.57 |
| A3 | 0.980 | 40.25 | 9.266 | 0.992 | 61.68 | 3.78 |

Table 4. Thermal kinetic results for pure and modified chitosan second region of pyrolysis.

| DM | <i>Pure chitosan</i> | | | <i>Chitosan-N-Phenylacetamide</i> | | |
|-----------|----------------------|-------------------------|---------------------------|-----------------------------------|-------------------------|---------------------------|
| | R ² | E _a (kJ/mol) | Ln A (min ⁻¹) | R ² | E _a (kJ/mol) | Ln A (min ⁻¹) |
| F1 | 0.845 | 9.262 | 13.88 | 0.917 | 8.523 | 13.875 |
| F2 | 0.894 | 39.919 | 8.745 | 0.919 | 33.563 | 9.512 |
| F3 | 0.906 | 77.316 | 1.168 | 0.923 | 63.198 | 2.629 |
| R3 | 0.974 | 15.719 | 13.173 | 0.989 | 15.367 | 13.190 |
| D3 | 0.430 | 1.899 | 13.814 | 0.599 | 1.857 | 13.766 |

3.4.4. Determination of the most probable reaction function.

In order to find the kinetic model of thermal degradation, the Criado and Coats–Redfern methods were chosen as they involve the degradation mechanisms. Coats–Redfern method was used. According to Eq. (4), the activation energy for every *g*(α) function listed in

table 1 can be calculated for all heating rates from fitting $\ln(g(\alpha)/T^2)$ versus $1/T$ plots. The activation energies and correlations are summarized in Tables 3 and 4, respectively, for the first and second degradation regions for both pure chitosan and chitosan-*N*-phenylacetamide.



Figure 8. Compensation effect $\ln A=f(E_a)$ for first and second regions of thermal degradation.

According to the Coats Redfern equation, if a correct model is selected for the reaction, the plot of $\ln(g(\alpha)/T^2)$ versus $1/T$ will be linear as possible with a high correlation coefficient. One can say that the Coats Redfern method reliability is not enough and cannot be used to kinetics assessment of reactions. From this point of view, the use of the method of Criado is very important; this method gives us more information and can be added to the Coats Redfern method.

The used models and the expressions of associated functions $g(x)$ and $f(x)$ are shown in Table 1. The master curve plots $Z(x)/Z(0.5)$ versus α for different mechanisms according to the Criado method for both pure chitosan and chitosan-*N*-phenylacetamide degradation is illustrated in figure 9. As can be seen, the comparison of the experimental master plots with theoretical ones revealed that the kinetic process for the degradation of both pure chitosan and chitosan *N*-phenylacetamide was most probably described by the reaction order F2. Thus, reaction order, order-based models (F_n) are the simplest models as they are similar to those used in homogeneous kinetics. In these models, the reaction rate is proportional to concentration, amount, or fraction remaining of reactant raised to a particular power, which is the reaction order.

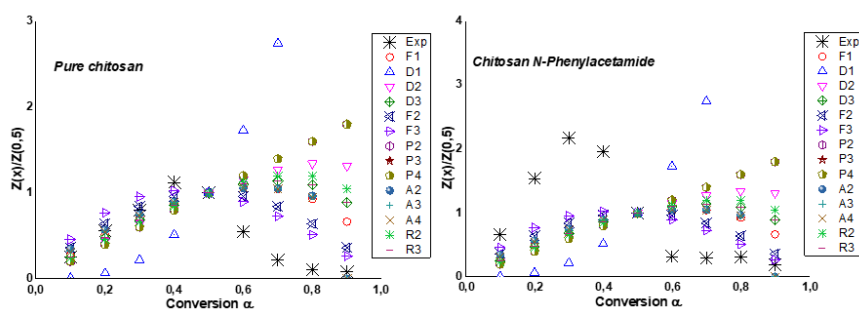


Figure 9. Masterplots of different kinetic models and experimental data at 20 Kmin^{-1} calculated by Eq. (5) for pure chitosan and chitosan-*N*-Phenylacetamide degradation.

4. Conclusion

In the present work, chitosan-*N*-phenylacetamide derivative was synthesized by the reaction of chitosan with 2-Chloro-*N*-phenylacetamide in an IL [Bmim](Cl) and characterized by IR spectroscopic techniques, XRD and SEM. Pure chitosan and chitosan-*N*-phenylacetamide were subjected to thermo-gravimetric analysis under an inert atmosphere in the temperature range of room temperature - $600 \text{ }^\circ\text{C}$ at a heating rate of $20 \text{ }^\circ\text{C}/\text{min}$ in order to

approach the mechanisms and kinetics of their thermal degradation. TGA and DTG temperature dependencies were explained. Decomposition processes proceed in three main stages: water evaporation, active and passive pyrolysis. TGA curves indicate that the active pyrolysis of pure and modified chitosan is between 240–380 °C. The stability of the synthesized product was evaluated, and the activation energy of degradation was calculated using the Coats–Redfern method. The thermal stability decreased by introducing *N*-phenylacetamide group compared to pure chitosan; this is evidence of significant chemical modification of chitosan and the formation of a chemical bond between these compounds, confirming that the reaction has occurred. Finally, Coats-Redfern and Criado methods were successfully utilized to predict the reaction mechanism of thermal degradation of both pure chitosan and chitosan-*N*-phenylacetamide. The pyrolysis reaction models of both pure chitosan and chitosan-*N*-phenylacetamide are described by second-order reaction (F2).

Funding

This research received no external funding

Acknowledgments

This research has no acknowledgment.

Conflicts of Interest

The authors declare no conflict of interest.

References

1. Majeti, N.V.; Kumar, R. A review of chitin and chitosan applications. *React. Funct. Polym.* **2000**, *46*, 1–27, [https://doi.org/10.1016/S1381-5148\(00\)00038-9](https://doi.org/10.1016/S1381-5148(00)00038-9).
2. Ullah, F., Javed, F., Khan, A.N., Abdul Kudus, M.H., Jamila, N., Minhaz, A., Akil, H.M. Synthesis and surface modification of chitosan built nanohydrogel with antiviral and antimicrobial agent for controlled drug delivery. *Biointerface Res. Appl. Chem.* **2019**, *9*, 4439–4445, <https://doi.org/10.33263/BRIAC96.439445>.
3. Kenawy, E.R.; Ali, S.S.; Al-Etewy, M.; Sun, J.; Wu, J.; El-Zawawy, N. Synthesis, characterization and biomedical applications of a novel Schiff base on methyl acrylate-functionalized chitosan bearing *p*-nitrobenzaldehyde groups. *Int. J. Biol. Macromol.* **2019**, *122*, 833–843, <https://doi.org/10.1016/j.ijbiomac.2018.11.005>.
4. Cristina, C.; Dolores, V.P.; Maria, R.G.; Siyuan, D.; Roberta, C.; Piera, D.M. Chitin and Chitosans: Characteristics, Eco-Friendly Processes, and Applications in Cosmetic Science. *Mar. Drugs.* **2019**, *17*, <https://doi.org/10.3390/md17060369>.
5. Amanzadi, B.; Mirzaei, E.; Hassanzadeh, G.; Mahdavian, P.; Boroumand, S.; Abdollahi, M.; Abdolghaffari, A.H.; Majidi R.F. Chitosan-based layered nanofibers loaded with herbal extract as wound-dressing materials on wound model studies. *Biointerface Res. Appl. Chem.* **2019**, *9*, 3979 – 3986 <https://doi.org/10.33263/BRIAC94.979986>.
6. Je, J.Y.; Kim, S.K. Chitosan derivatives killed bacteria by disrupting the outer and inner membrane. *J. Agric. Food Chem.* **2006**, *54*, 6629–6633, <https://doi.org/10.1021/jf061310p>.
7. Paldurețu, C. C.; Apetroaei, M. R.; Rău, I.; Schroder, V. Characterization of chitosan extracted from different romanian black sea crustaceans. *UPB Sci. Bull. Ser. B Chem. Mater. Sci.* **2018**, *80*, 13–24.
8. Dutta, P.K.; Dutta, J.; Tripathi, V.S. Chitin and chitosan: Chemistry, properties and applications. *J. Sci. Ind. Res.* **2004**, *63*, 20–31.
9. Aranaz, I.; Mengibar, M.; Harris, R.; Panos, I.; Miralles, B.; Acosta, N.; Galed, G.; Heras, A. Functional characterization of chitin and chitosan. *Curr. Chem. Biol.* **2009**, *3*, 203–30 <https://doi.org/10.2174/187231309788166415>.
10. Kenawy, E.R.; Abdel-Hay, F.I.; Tamer, T.M.; Abo-Elghit Ibrahim, E.M.; Mohy Eldin, M.S. Antimicrobial activity of novel modified aminated chitosan with aromatic esters. *Polym. Bull.* **2020**, *77*, 1631–1647, <https://doi.org/10.1007/s00289-019-02816-w>.

11. Aljafree, N.F.A.; Kamari, A. Synthesis, characterisation and potential application of deoxycholic acid carboxymethyl chitosan as a carrier agent for rotenone. *J. Polym. Res.* **2018**, *25*, <https://doi.org/10.1007/s10965-018-1530-6>.
12. Malekshah, R.E.; Shakeri, F.; Khaleghian, A.; Salehi, M. Developing a biopolymeric chitosan supported Schiff-base and Cu(II), Ni(II) and Zn(II) complexes and biological evaluation as pro-drug. *Int. J. Biol. Macromol.* **2020**, *152*, 846–861, <https://doi.org/10.1016/j.ijbiomac.2020.02.245>.
13. Hemming, E.B.; Masters, A.F.; Perosa, A.; Selva, M.; Maschmeyer, T. Single-Step Methylation of Chitosan Using Dimethyl Carbonate as a Green Methylating Agent. *Molecules* **2019**, *24*, <https://doi.org/10.3390/molecules24213986>.
14. Antony, R.; Arun, T.; Manickam, S.T.D. A review on applications of chitosan-based Schiff bases. *Int. J. Biol. Macromol.* **2019**, *129*, 615–633, <https://doi.org/10.1016/j.ijbiomac.2019.02.047>.
15. Mohy Eldin, M.S.; Hashem, A.I.; Omer, A.M.; Tamer, T.M. Preparation, characterization and antimicrobial evaluation of novel cinnamyl chitosan Schiff base. *Int. J. Adv. Res.* **2015**, *3*, 741-755.
16. Kubisa, P. Application of ionic liquids as solvents for polymerization processes. *Prog. Polym. Sci.* **2004**, *29*, 3–12, <https://doi.org/10.1016/j.progpolymsci.2003.10.002>.
17. Singh, B.; Sekhon, S.S. Polymer electrolytes based on room temperature ionic liquid: 2,3-dimethyl-1-octylimidazolium triflate. *J. Phys. Chem. B* **2005**, *109*, 16539–16543, <https://doi.org/10.1021/jp051673c>.
18. Huddleston, J.G.; Visser, A.E.; Reichert, W.M.; Willauer, H.D.; Broker, G.A.; Rogers, R.D. Characterization and comparison of hydrophilic and hydrophobic room temperature ionic liquids incorporating the imidazolium cation. *Green Chem.* **2001**, *3*, 156–164, <https://doi.org/10.1039/B103275P>.
19. Zhu, S.D.; Wu, Y.X.; Chen, Q.M.; Yu, Z.N.; Wang, C.W.; Jin, S.W.; Ding, Y.; Wu, G. Dissolution of cellulose with ionic liquids and its application: a mini review. *Green. Chem.* **2006**, *8*, 325-327, <https://doi.org/10.1039/B601395C>.
20. Zhang, H.; Wu, J.; Zhang, J.; He, J.S. 1-Allyl-3-methylimidazolium chloride room temperature ionic liquid: a new and powerful nonderivatizing solvent for cellulose. *Macromolecules* **2005**, *38*, 8272–8277, <https://doi.org/10.1021/ma0505676>.
21. El Hamdaoui, L.; El Moussaouiti, M.; Gmouh, S. Homogeneous esterification of cellulose in the mixture n-butylpyridinium chloride/dimethylsulfoxide. *International Journal of Polymer Science* **2016**, *2016*, <https://doi.org/10.1155/2016/1756971>.
22. Xie, H.B.; Zhang, S.B.; Li, S.H. Chitin and chitosan dissolved in ionic liquids as reversible sorbents of CO₂. *Green. Chem.* **2006**, *8*, 630-633, <https://doi.org/10.1039/B517297G>.
23. Stefanescu, C.; Daly, W.; Negulescu, I. 1-Butyl-3-Methylimidazolium Acetate as a Solvent Media for Functionalization of Chitosan. *Polymer Prepr.* **2009**, *50*, 143-144.
24. Stefanescu, C.; Daly, W.; Negulescu, I. Nucleophilic Reactivity of Chitosan in Ionic Liquids Promoted by Tert-Amines. *Polymer Prepr.* **2009**, *50*, 551-552.
25. Saniyat, I.; Arnold, L.; Padhye, R. Comparison and Characterisation of Regenerated Chitosan from 1-Butyl-3-methylimidazolium Chloride and Chitosan from Crab Shells. *BioMed. Res. Int.* **2015**, *2015*, *6*, <http://dx.doi.org/10.1155/2015/874316>.
26. Brown, M.E. *Introduction to Thermal Analysis: Techniques and Applications*. 2nd Ed. New York: Springer, **2001**.
27. Salama, H.E.; Saad, G.R.; Sabaa, M.W. Synthesis, characterization and biological activity of Schiff bases based on chitosan and arylpyrazole moiety. *Int. J. Biol. Macromol.* **2015**, *79*, 996–1003, <https://doi.org/10.1016/j.ijbiomac.2015.06.009>.
28. Vasilev, A.; Efimov, M.; Bondarenko, G.; Kozlov, V.; Dzidziguri, E.; Karpacheva, G. Thermal behavior of chitosan as a carbon material precursor under IR radiation. *IOP Conf. Ser.: Mater. Sci. Eng.* **2019**, *693*, <https://doi.org/10.1088/1757-899X/693/1/012002>.
29. Lal, S.; Arora, S.; Kumar, V.; Rani, S.; Sharma, C.; Kumar, P. Thermal and biological studies of Schiff bases of chitosan derived from heteroaryl aldehydes. *Journal of Thermal Analysis and Calorimetry* **2018**, *132*, 1707-1716, <https://doi.org/10.1007/s10973-018-7147-5>.
30. Ou, C.Y.; Zhang, C.H.; Li, S.D.; Yang, L.; Dong, J.J.; Mo, X.L.; Zeng, M.T. Thermal degradation kinetics of chitosan–cobalt complex as studied by thermogravimetric analysis. *Carbohydr. Polym.* **2010**, *82*, 1284–1289, <https://doi.org/10.1016/j.carbpol.2010.07.010>.
31. Katke, S.A.; Amrutkar, S.V.; Bhor, R.J.; Khairnar, M.V. Synthesis of biologically active 2-chloro-n-alkyl/aryl acetamide derivatives. *International Journal of Pharma Sciences and Research* **2011**, *2*, 148-156.
32. Duckworth, C.A. *Stable emulsion flowable formulation of a 2-chloroacetamide herbicide and an imidazolone herbicide*. US patent: 5, **1995**; pp. 538-938.
33. El Hamdaoui, L.; Talbaoui, A.; El Moussaouiti, M. Synthesis and characterization of cellulose-acetanilide ether and its antibacterial activity. *Polym Bull.* **2018**, *75*, 2401–2413, <https://doi.org/10.1007/s00289-017-2164-2>.
34. Lu, Z.X.; Yuan, X.; Wu, J.; Wang, L.J.; Luo, H.A. Synthesis and spectroscopic characterization of N, N'-dialkylimidazolium-based ionic liquids. *Chemical World.* **2005**, *46*, 148-150.
35. Criado, J.M.; Málek, J.; Ortega, A. Applicability of the master plots in kinetic analysis of non-isothermal data. *Thermochim Acta.* **1989**, *147*, 377-385, [https://doi.org/10.1016/0040-6031\(89\)85192-5](https://doi.org/10.1016/0040-6031(89)85192-5).

36. Núñez, L.; Fraga, F.; Núñez, M.R.; Villanueva, M. Thermogravimetric study of the decomposition process of the system BADGE (n = 0)/1, 2 DCH. *Polymer*. **2000**, *41*, 4635-4641, [https://doi.org/10.1016/S0032-3861\(99\)00687-4](https://doi.org/10.1016/S0032-3861(99)00687-4).
37. Dickinson, C.F.; Heal, G.R. A review of the ICTAC kinetic project, 200 – Part 1, Nonisothermal results. *Thermochim. Acta*. **2009**, *494*, 15-25.
38. Bustamante, V.L.; Rogaume, T.; Guillaume, E.; Rein, G.; Torero, J.L. Analysis of principal gas products during combustion of polyether polyurethane foam at different irradiance levels. *Fire Safety J.* **2009**, *44*, 933-940, <https://doi.org/10.1016/j.firesaf.2009.05.003>.
39. Valensi, G. Analysis of the methods of interpreting reactions of a gas with a solid to form another solid. *J Chim Phys.* **1950**, *47*, 489-505.
40. Jander, W.; Anorg Z. Reactions in solid-state at high temperatures. *U. Allgemeine Chemie* **1927**, *163*, 1-30.
41. Ginstling, A.M.; Braustein, B.I.; Zhurnal, P.K. Concerning the diffusion kinetics of reactions in spherical particles. *J. Appl. Chem. USSR.* **1950**, *23*, 1327-1338.
42. Avrami, M. Kinetics of phase change, General theory. *J. Chem. Phys.* **1939**, *7*, <https://doi.org/10.1063/1.1750380>.
43. Erofeev, B.V. *Comptes Rendus de l'Académie des Sciences URSS.* **1940**; pp. 52.
44. Coats, A.W. Redfern, J.P. Thermogravimetric analysis: A review. *Analyst* **1963**, *88*, 906-924, <https://doi.org/10.1039/AN9638800906>.
45. Coats, A.W.; Redfern, J.P. Kinetic parameters from the thermogravimetric data. *Nature (London)* **1964**, *201*, 68-69, <https://doi.org/10.1038/201068a0>.
46. Criado, J.M. Kinetic analysis of DTG data from master curves. *Termochim Acta.* **1978**, *24*, 186-189, [https://doi.org/10.1016/0040-6031\(78\)85151-X](https://doi.org/10.1016/0040-6031(78)85151-X).
47. Kumar, S.; Dutta, P.K.; Koh, J. A physico-chemical and biological study of novel chitosan-chloroquinoline derivative for biomedical applications. *Int. J. Biol. Macromol.* **2011**, *49*, 356-361, <https://doi.org/10.1016/j.ijbiomac.2011.05.017>.
48. Zhang, Y.; Xue, C.; Xue, Y.; Gao, R.; Zhang, X. Determination of the degree of deacetylation of chitin and chitosan by X-ray powder diffraction. *Carbohydr. Res.* **2005**, *340*, 1914-1917, <https://doi.org/10.1016/j.carres.2005.05.005>.
49. Jiao, T.F.; Zhou, J.; Zhou, J.; Gao, L.; Xing, Y.; Li, X. Synthesis and Characterization of Chitosan-based Schiff Based Compounds with Aromatic Substituent Group. *Iran. Polym. J.* **2011**, *20*, 123-136.
50. Lomadze, N.; Schneider, H.J. A chitosan-based chemomechanical polymer triggered by stacking effects with aromatic effectors including aminoacid derivatives. *Tetrahedron.* **2005**, *61*, 8694-8698, <https://doi.org/10.1016/j.tet.2005.06.092>.
51. Walter, G.K. Le matériau bois-proprétés technologie. Mise en œuvre. *Association pour la recherche sur le bois en Lorraine* **1983**.
52. Wanjun, T.; Cunxin, W.; Donghua, C. Kinetic studies on the pyrolysis of chitin and chitosan. *Polym. Degrad. Stab.* **2005**, *87*, 389-394, <https://doi.org/10.1016/j.polymdegradstab.2004.08.006>.
53. De Britto, D.; Campana-Filho, S.P. Kinetics of thermal degradation of chitosan. *Thermochim. Acta.* **2007**, *465*, 73-82, <https://doi.org/10.1016/j.tca.2007.09.008>.
54. Lopez, F.A.; Merce, A.L.R.; Alguacil, F.J.; Lopez-Delgado, A. A kinetic study on the thermal behaviour of chitosan. *J. Ther. Anal. Cal.* **2008**, *91*, 633-639, <https://doi.org/10.1007/s10973-007-8321-3>.